Heliyon 9 (2023) e18757

Contents lists available at ScienceDirect

Heliyon

journal homepage: www.cell.com/heliyon

Evaluation of the time-dependent osteogenic activity of glycerol incorporated magnesium oxide nanoparticles in induced calvarial defects

Ghada H. Naguib [a,b,*], Gamal S. Abd El-Aziz [c], Ahmad Almehmadi [d], Amr Bayoumi [e], Abdulghani I. Mira [f], Ali Habiballah Hassan [g], Mohamed T. Hamed [h,i]

[a] Department of Restorative Dentistry, Faculty of Dentistry, King Abdulaziz University, Jeddah, Saudi Arabia
[b] Department of Oral Biology, Cairo University School of Dentistry, Cairo, Egypt
[c] Department of Clinical Anatomy, Faculty of Medicine, King Abdulaziz University, Jeddah, Saudi Arabia
[d] Department of Oral Biology, Faculty of Dentistry, King Abdulaziz University, Jeddah, Saudi Arabia
[e] Department of Oral and Maxillofacial Surgery, Faculty of Dentistry, King Abdulaziz University, Jeddah, Saudi Arabia
[f] Department of Restorative Dentistry, King Abdulaziz University, Jeddah, Saudi Arabia
[g] Department of Orthodontics, King Abdulaziz University, Jeddah, Saudi Arabia
[h] Department of Oral and Maxillofacial Prosthodontics, Faculty of Dentistry, King Abdulaziz University, Jeddah, Saudi Arabia
[i] Department of Fixed Prosthodontics, Cairo University School of Dentistry, Cairo, Egypt

ARTICLE INFO

Keywords:
MgO nanoparticles
Glycerol
Bone healing
Calvarial defect
Histopathology
Micro-CT

ABSTRACT

Introduction: Magnesium-based biomaterials have been explored for their potential as bone healing materials, as a result of their outstanding biodegradability and biocompatibility. These characteristics make magnesium oxide nanoparticles (MgO NPs) a promising material for treating bone disorders. The purpose of this investigation is to assess the osteogenic activity of newly-developed locally administered glycerol-incorporated MgO NPs (GIMgO NPs) in rabbits' calvarial defects.

Materials and methods: Characterization of GIMgO was done by X-ray Diffraction (XRD) and Fourier Transform Infrared Spectroscopy (FTIR). Bilateral calvarial defects were created in eighteen New Zealand Rabbits, of which they were divided into 3 groups with time points corresponding to 2, 4, and 6 weeks postoperatively (n = 6). One defect was implanted with absorbable gel foam impregnated with GIMgO NPs while the other was implanted with gel foam soaked with glycerol (the control). The defects were assessed using histological, Micro-Computed Tomography (Micro-CT), and histometric evaluation.

Results: The characterization of the GIMgO nanogel revealed the presence of MgO NPs and glycerol as well as the formation of the crystalline phase of the MgO NPs within the nanogel sample. The histological and micro-CT analysis showed time-dependent improvement of healing activity in the calvarial defects implanted with GIMgO NPs when compared to the control. Furthermore, the histometric analysis demonstrated a marked increase in the total area of new bone, connective tissue, new bone area and volume in the GIMgO NPs implanted site.

Abbreviations: GIMgO NPs, Glycerol Incorporated Magnesium Oxide Nanoparticles; NPs, Nanoparticles; MgO, Magnesium oxide; MgO NPs, Magnesium oxide nanoparticles; NBF, Neutral buffer formalin; XRD, X-ray diffraction; FTIR, Fourier Transform Infrared spectroscopy; Micro-CT, Micro computed tomography; TA, Total area; NBA, New bone area; NBV, New bone volume.

* Corresponding author. Department of Restorative Dentistry, Faculty of Dentistry, King Abdulaziz University, Jeddah, Saudi Arabia.
E-mail addresses: gnagieb@kau.edu.sa, ghadanaguib905@yahooo.com (G.H. Naguib), mthamed@kau.edu.sa (M.T. Hamed).

https://doi.org/10.1016/j.heliyon.2023.e18757
Received 5 May 2023; Received in revised form 6 July 2023; Accepted 26 July 2023
Available online 27 July 2023

Statistically, the amount of new bone formation was more significant at 6 weeks than at 2 and 4 weeks postoperatively in the calvarial defects implanted with GIMgO NPs as compared to the control.
Conclusion: The locally applied GIMgO NPs demonstrated efficacy in promoting bone formation, with more significant effects observed over an extended period. These findings suggest its suitability for clinical use as a therapeutic alternative to enhance bone healing.

1. Introduction

In the fields of oral, maxillofacial, and reconstructive surgery, the dilemma of bone repair deserves significant attention, particularly in patients affected by large bone defects as a result of congenital, pathological, or traumatic causes. These extensive bone defects are unable to undergo self-healing and often result in delayed union, nonunion, or malunion, contributing to a high incidence of disability and deformity [1]. Additionally, several factors such as aging, radiotherapy, certain medications, and chronic diseases like osteoporosis and diabetes can disrupt the ability of bones to heal [2,3].

In this regard, several regenerative procedures have been proposed to support bone repair, with the primary objective focused on enhancing bone metabolism, bone induction, and osteogenesis. Many conventional techniques for bone repair involved replacing the missing or damaged bone with bone transplants, such as autografts and allografts [4,5]. However, these grafting implants were associated with several drawbacks, including the short supply of these grafts, immune rejection from the host, infection risks, prolonged healing duration, and high surgical procedure costs [6–8].

The advancements in the field of biomaterials and synthetic bone substitutes have facilitated the creation of bone implants capable of aiding in bone repair. These substitutes have gained popularity in the treatment of bone defects due to their ability to obviate the need for biological tissues and additional surgical sites, while also eliciting minimal immune response from the host [9,10]. However, it is important to note that several of these materials exhibit limited bioactivity and osteogenic capabilities [11].

The advent of nanotechnology has facilitated the development of nanostructures that mimic the natural bone's structures and sizes [12]. Nanomaterials possess distinctive physical and chemical properties, making them highly desirable for applications throughout various fields, including medicine, electronics, energy, and the environment. The physical and chemical characteristics of nanomaterials are influenced by factors such as size, shape, composition, and surface properties [13]. In particular, size plays a crucial role, resulting in a significantly larger surface area as well as an increased reactivity compared to their bulkier counterparts. Nanoparticles can take on various shapes, ranging from spherical, rod-like, or triangular to more intricate forms, which can impact their performance, including their dispersibility in liquid environments [14,15].

In recent times, the introduction of nanostructured biomaterials, such as nanostructured ceramics and nanobiogels, has demonstrated significant improvements in achieving bone healing. Studies have reported that these nanomaterials mimic the nanocharacteristics of bone, resulting in enhanced bone reconstruction [16]. However, these biomaterials demonstrate certain limitations such as poor mechanical strength or inadequate degradation rates [17].

Metal and metal oxide nanoparticles (NPs) have gained significant attention in the field of bone regeneration due to their unique properties and potential applications. Metal NPs, such as silver, gold, and titanium, possess antimicrobial properties that can prevent infections and promote bone healing [18,19]. These NPs can also stimulate osteoblast activity and enhance mineralization processes [20]. Among these oxides, magnesium oxide (MgO) has garnered special interest due to its potential for bone repair and bactericidal effects [21,22]. MgO has been proven to positively influence the differentiation and proliferation of bone cells, expediting bone regeneration [23]. Furthermore, there has been an increasing incorporation of MgO NPs into polymer composites and biomedical implants in recent years. This is primarily due to the MgO NPs' ability to enhance the mechanical properties of these materials, in addition to their potential as bone healing agents as a result of the exceptional biodegradability and biocompatibility of MgO [24–26].

Nevertheless, challenges related to biocompatibility and efficient delivery systems need to be addressed for their successful translation into clinical applications [27]. According to the aforementioned data, we designed this research to evaluate the bone healing activity of newly-developed locally implanted glycerol-incorporated MgO nanogel formulation in experimentally created calvarial defects in rabbits.

2. Materials and Methods

2.1. Chemicals

Magnesium oxide nanoparticles (MgO NPs) [nano-powder, $\leq$50 nm particle size (BET)], glycerol (pharmaceutical grade 99.5%), gel foam, and all other chemicals used in this study were purchased from Sigma-Aldrich chemical company (St. Louis, USA).

2.2. Preparation of glycerol incorporated magnesium oxide nanoparticles (GIMgO NPs)

The GIMgO NPs 1% w/w solution was prepared by suspending 1 gm of MgO NPs with 99 gm of glycerol under aseptic condition. Sonication was performed to disperse NPs using a probe sonicator (BioLogics, Inc., Manassas, Virginia, USA) for 10 min [28,29].

2.3. Characterization of MgO NPs

2.3.1. X-Ray Diffraction (XRD)

The diffraction pattern of the GIMgO NPs was done using an X-ray diffractometer (XRD) (Rigaku, Ultima IV, Japan) in order to study the type of phases and crystalline structure of MgO NPs. The source of radiation was Cu-kα with wavelength λ = 1.5406 Å, current of 30 mA, and voltage of 40 kV. The XRD spectra were scanned in the 2θ range of 10–80°.

2.3.2. Fourier Transform Infrared Spectroscopy (FTIR)

The FTIR analysis of the GIMgO NPs was investigated using PerkinElmer Spectrum 1000 spectrum (Shelton, CT, USA) by utilizing K Br plates in the absorbance mode at a wave number range of 600–4000 cm^{-1}.

2.4. Loading of GIMgO NPs on pieces of gel foam

Pieces of gel foam (5 × 5 mm) were soaked in the freshly prepared GIMgO NPs for 1 min and used immediately in the tested bony defects.

2.5. Animals and experimental design

Eighteen adult male New Zealand rabbits with an average weight of 3.75 kg were used in this study. All animals were housed in the animal unit at King Fahad Medical Research center in King Abdulaziz University, Jeddah, Saudi Arabia. The rabbits were individually housed in cages with free access to food and water ad libitum. The care and experimental protocols were accomplished in compliance with the "Guide for the Care and Use of Laboratory Animals". Rabbits were split into three groups (n = 6) according to the follow-up period as follows:

- Group 1: subjected to the surgical procedure and sacrificed after 2 weeks.
- Group 2: subjected to the surgical procedure and sacrificed after 4 weeks.
- Group 3: subjected to the surgical procedure and sacrificed after 6 weeks.

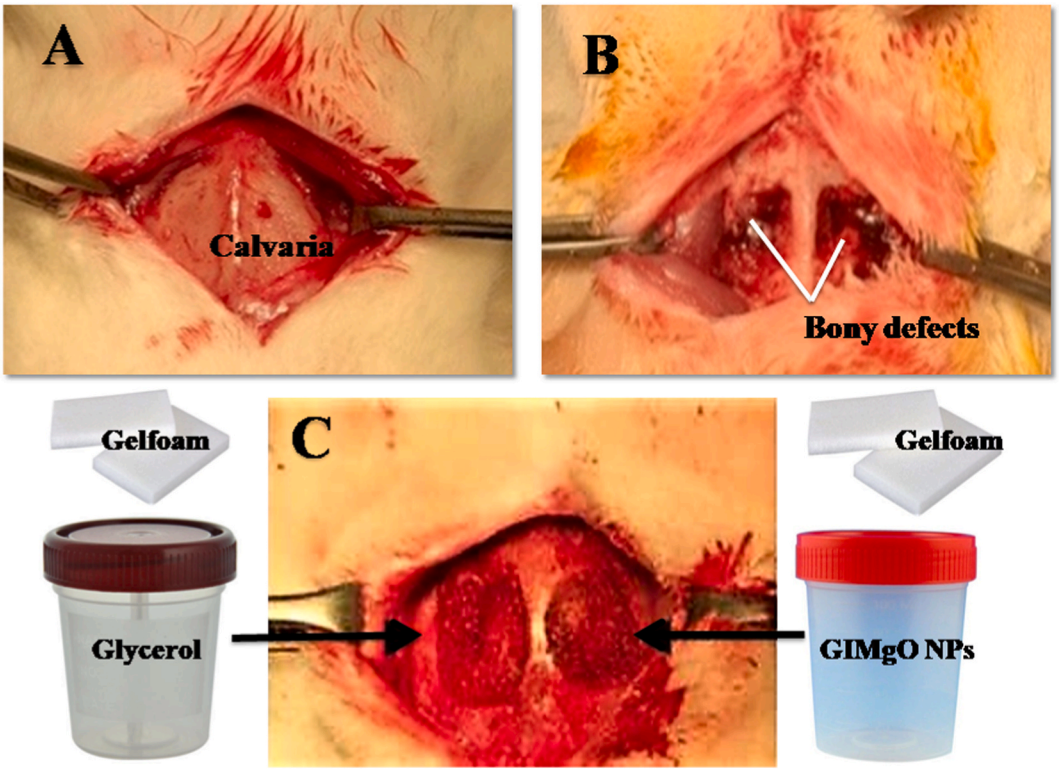

Fig. 1. Showing the surgical steps. A: exposure of the calvaria; B: creation of circular bony defects with intact dura matter; C: filling the defects with the GIMgO NPs soaked gel foam on one side (tested site) and glycerol gel foam on the other side (control site).

2.6. Surgical procedure

All procedures were performed in a surgical operating room under sterile conditions according to previous studies [30,31]. After overnight fasting, each rabbit was anesthetized by an intramuscular injection with a mixture of ketamine (5 mg/kg) and acepromazine (1.5 mg/kg) and given preoperative antibiotic (enrofloxacin 5 mg/kg subcutaneously). Then, the rabbit was fixed on a surgical table in a prone position. After shaving the calvaria skin and disinfecting it with alcohol, a longitudinal dissection along the sagittal suture was made in the scalp. Parietal bones were exposed by reflecting the skin, subcutaneous tissue, and periosteum. A critical size full-thickness defect measuring 7 mm in diameter was made on the left and right parietal bones using a low-speed trephine drill under constant cold saline irrigation, exposing the dura mater. Glycerol-soaked gel foam was implanted in one side (control site) and GIMgO NPs-soaked gel foam was implanted to other side (tested site). Then, a 4.0 silk suture was used to close the incision after readjusting the periosteum (Fig. 1). The rabbits recovered from anesthesia and were given postoperative anti-pain drugs and antibiotics.

2.7. Sample collection

At two, four, and six weeks, the rabbits of each group were sacrificed by a fatal intramuscular injection using a mixture of xylazine and ketamine hydrochloride. To obtain the bony specimens, the calvarial defects were identified and removed *enbloc* using a high-speed rotatory device with 3 mm of intact bone from the borders of the right and left holes to examine the normal bone structure.

2.8. Histological study

The halves of bony samples were fixed in 10% neutral buffer formalin (NBF) for 10 days and were decalcified in decal solution (Shandoon TBD-1^{M}, Thermo Scientific) for 14 days, after which they were embedded in paraffin parallel to the sectioned surface. Serial 5 μm thick sections were cut coronally along the midline of the calvarial defects and stained with hematoxylin-eosin (H & E) for histological and histometric analysis [32]. An Olympus light microscope (Olympus BX61- USA) with a built-in digital camera (Olympus 20) was utilized for microscopic examination and digital photomicrography (at magnifications of 40X and 100X).

Histometric analysis of the two calvarial defects for each rabbit was performed using Image-Pro Plus software (Media Cybernetics, Silver Spring), where 6 different pictures of each cross-section at 100X magnification were assessed according to previous studies (analysis system; Image J) [33]. The following parameters were measured in mm^2:

- Total area (TA) of new bone and connective tissue within the margins of the bony defects, including new mineralized bone and non-mineralized tissue.

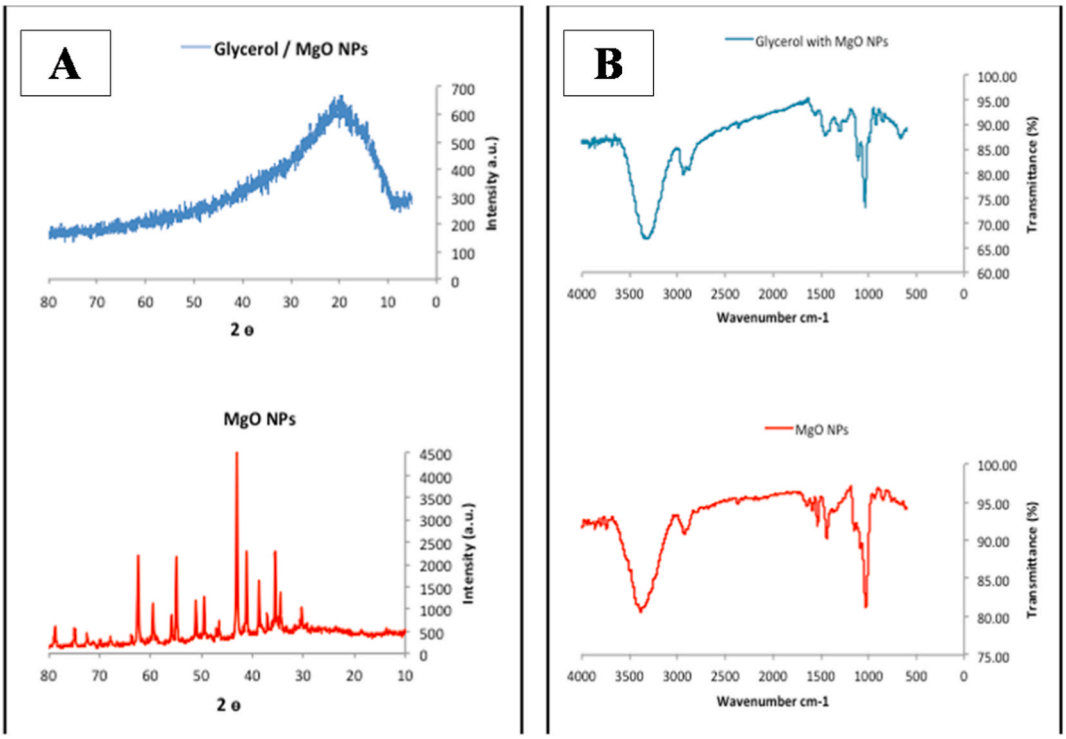

Fig. 2. A. XRD pattern of GIMgO NPs and MgO NPs. B. FTIR spectrum of the synthesized GIMgO NPs and MgO NPs.

- New bone area (NBA) of the newly formed bone that was regenerated within the margins of the bony defects.

2.9. Micro computed tomography (Micro-CT) study

The other halves of the bony specimens were prepared for micro-CT scan (Skyscan 1174, Skyscan, Belgium, Faculty of Dentistry, KAU) at 100 kV voltage, 100 mA current, and 2300 ms of exposure time. The captured X-ray projections were at 0.70° intervals and 180° angular rotation. The specimens were scanned with a 40 μm pixel size. 3-D images were composed by NRecon 1.66 computer software (Skyscan) assessing the continuous measurements of the bony defect axes (coronal, *trans*-axial, and sagittal). Micro-CT analysis of the two calvarial defects for each rabbit to assess the new bone volume (NBV in mm^3) was done according to a previous study [34].

2.10. Statistical analysis

The obtained histometric data from the calvarial defect samples were expressed as mean ± standard deviation (SD) values of groups. Analysis by one-way ANOVA using SPSS (version 21, Chicago, IL, USA) was performed to analyze the difference between the groups followed by Tukey's test. Statistical significance was considered when $P < 0.05$.

3. Results

3.1. Characterization of GIMgO NPs

3.1.1. XRD analysis

The XRD evaluation was conducted to determine the size, construction, and pureness of the GIMgO nanogel. The XRD profile showed various peaks, which matched those in the standard reference file in both angular location and intensity, confirming the formation of the crystalline phase of MgO NPs in the sample (Fig. 2A). Additionally, the small percentage of MgO NPs in the glycerol-based blends lead to a decrease in the crystallite size/area. There was no variation in the XRD peaks on inclusion of the MgO NPs to glycerol, revealing that the spatial interrelationship between the two organized zones underwent no considerable transformation.

3.1.2. FTIR analysis

FTIR was done to identify the function group and features of MgO NPs in the sample of GIMgO NPs. The samples were scanned at the range of wave numbers at 400 cm^{-1} to 4000 cm^{-1}. The spectra showed several peaks at different absorption bands, which indicated the presence of MgO NPs (Fig. 2B). At 1000 cm^{-1}, a slight shift and stretch of the band due to C–O bond of alcohol was seen, as well as a

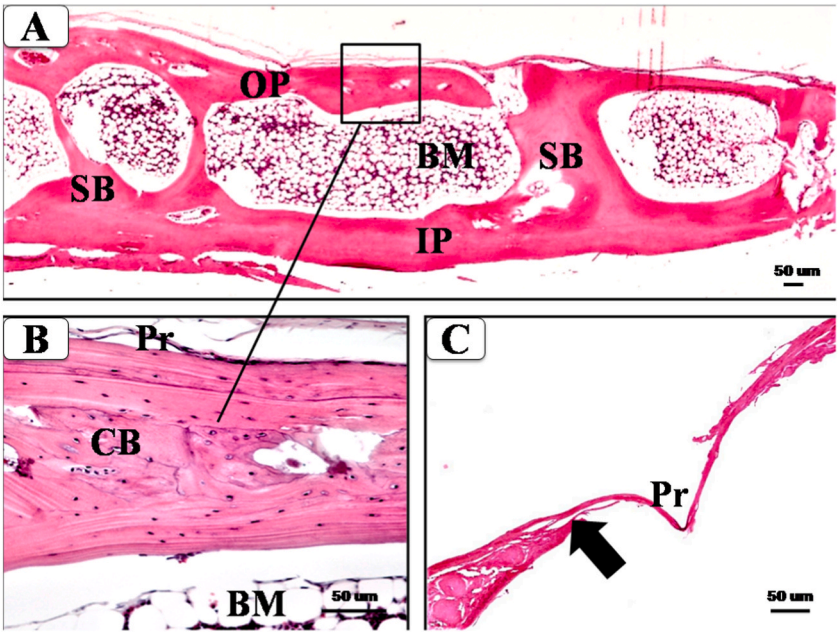

Fig. 3. Microscopic photomicrographs showing coronal sections of rabbit's calvaria before and after the surgical procedure. **A.** Normal calvarial wall, which is formed of outer (OP) and inner (IP) plates with bone marrow cavities (BM) in between (H&E x 40). **B.** Inset showing higher magnification of the outer calvarial plate, which is formed of compact bone (CB) covered by periosteum (Pr) (H&E x 200). **C.** Preservation of the periosteum (Pr) after removal of the calvarial defect (H&E x 100).

broadening of the peak at 1420 cm^{-1} related to the C–H bond. Two peaks attributed to the C–H bond were observed at 2880 cm^{-1} and 2940 $cm^{-1,}$ indicating the presence of glycerol in the reaction. Also, a shift of the band appeared at 2900 cm^{-1} as well as a stretching of the band at 3300 cm-1, due to the presence of O–H bundle of alcohol as a result of the intermolecular bond of the MgO NPs.

3.2. Histological results

The histological examination of the surgically removed bony part of the rabbit's calvaria (Fig. 3) showed a normal structure

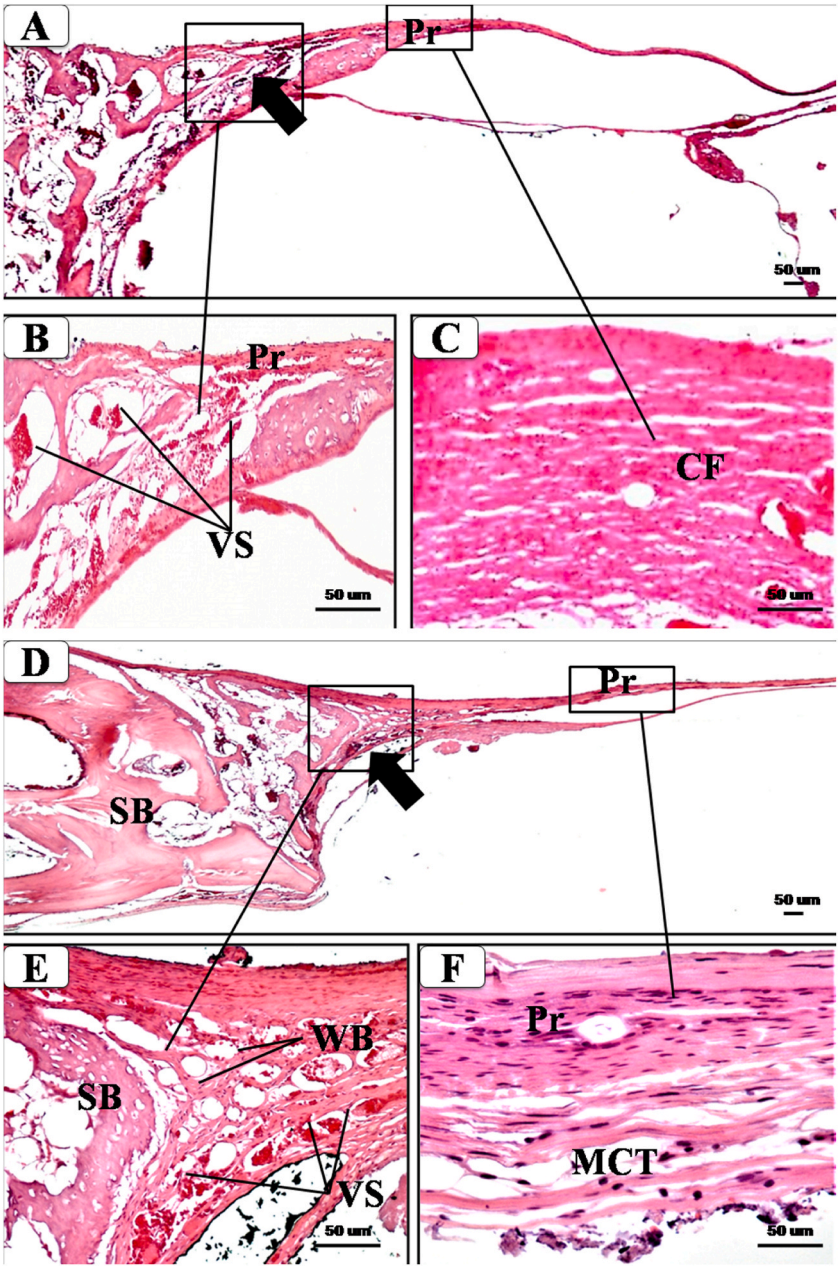

Fig. 4. Microscopic photomicrographs of rabbit's calvaria H&E-stained sections at two weeks after the surgical procedure showing: **Control Site (A, B, C): A.** Slightly thickened periosteum (Pr) with slightly enlarged lower peripheral edge of the defect (thick arrow). (x 40). **B.** Inset showing peripheral edge of the defect with small vascular spaces (VS). (x 200). **C.** Inset showing central part of the defect with condensation of wavy collagen fibers (CF), which come from the underlying surface of the periosteum (Pr). (x 200). **Treated site (D, E, F): D.** More thickened periosteum (Pr) with enlarged lower peripheral edge of the defect (thick arrow), SB = spongy bone of nearby part of native bone. (x 40) **E.** Inset of peripheral edge of the defect margin with more vascular spaces (VS) and appearance of new woven bone formation (WB). (x 200) **F.** Inset of central part of the defect was filled with thickened periosteum (Pr) with appearance of several layers of mesenchymal (undifferentiated) connective tissue (MCT). (x 200).

comprising of two plates (outer and inner) of compact bone with a layer of spongy bone in between (diploë) as indicated by the presence of bony trabeculae and bone marrow cavities.

At 2 weeks, the central part of the defect in the control site (Fig. 4 A, B, C) showed a slightly thickened periosteum with condensation of wavy collagen bundles, which seemed to come from the underlying surface of the periosteum. At the peripheral edge of the defect, there was the appearance of some vascular spaces. No evidence of new bone formation could be detected. In the defect site implanted with GIMgO NPs (test site) (Fig. 4 D, E, F), the central part of the defect displayed thickening of the periosteum with

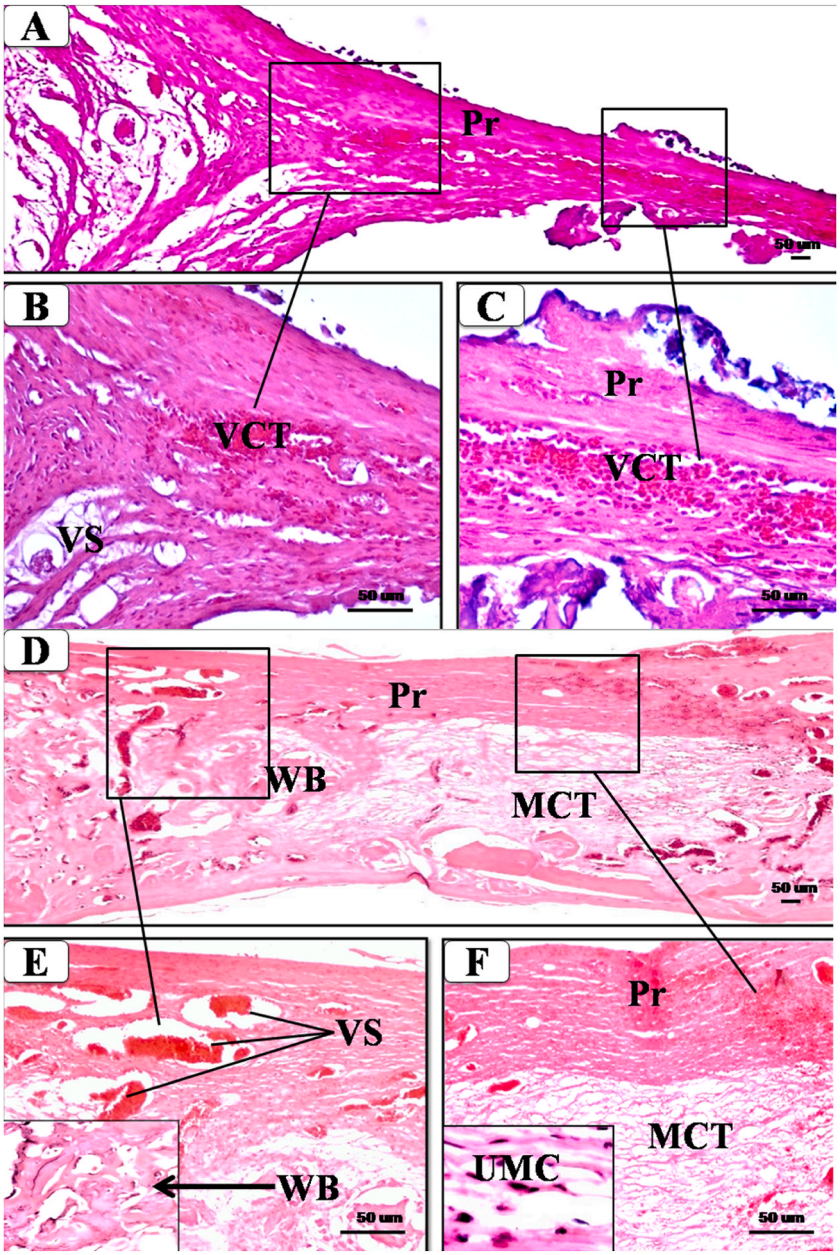

Fig. 5. Microscopic photomicrographs of rabbit's calvaria H&E-stained sections at four weeks after the surgical procedure showing: **Control Site (A, B, C): A.** More thickened periosteum (Pr) with enlarged lower peripheral edge of the defect and appearance of vascularized connective tissue. (x 40). **B.** Inset of peripheral edge of the defect showing more vascular spaces (VS) and vascularized connective tissue (VCT) with no evidence of new bone formation (NBF). (x 200). **C.** Inset of central part of the defect showing thickened and condensed layers of Pr with wider layer of VCT. (x 200). **Treated site (D, E, F): D.** More thickened periosteum (Pr) with appearance of mesenchymal connective tissue (MCT), and the presence of large vascular spaces and woven bone (WB). (x 40) **E.** Inset of peripheral edge of the defect margin showing NBF in the form of small and irregular spicules of woven bone (WB) [lower left inset]. (x 200). **F.** Inset of central part of the defect showing thickened Pr with appearance of several layers of mesenchymal connective tissue (MCT) which contained undifferentiated mesenchymal cells (UMC) [lower left inset]. (x 200).

appearance of several layers of mesenchymal (undifferentiated) connective tissue deriving from its underlying surface. At the margins of the defect adjacent to the native bone, additional vascular spaces as well as the appearance of a new woven bone arrangement were recognized.

At 4 weeks, the boundary of the defect area in the control site (Fig. 5 A, B, C) showed more vascular spaces and vascularized connective tissue with no evidence of new bone formation. In the central part of the defect, there were thickened and condensed layers of the periosteum with a wider layer of vascularized connective tissue. In the defect site implanted with the GIMgO NPs (test site)

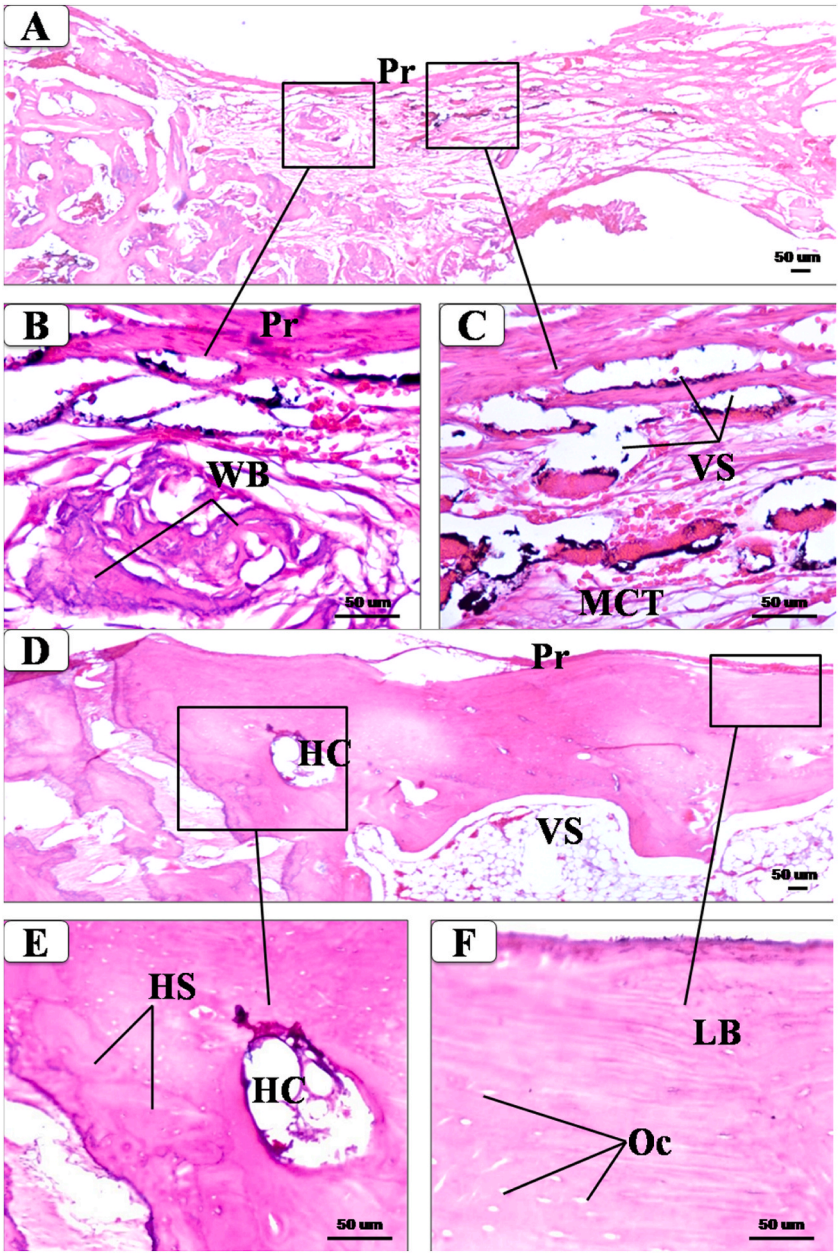

Fig. 6. Microscopic photomicrographs of rabbit's calvaria H&E-stained sections at six weeks after the surgical procedure showing: **Control Site: A.** Mesenchymal connective tissue, large vascular spaces and newly formed woven bone that occupied nearly all the defect site under the periosteum (Pr). (40). **B.** Inset of peripheral edge of the defect margin showing a new bone formation in the form of small and irregular spicules of woven (immature) bone (WB) with presence of large vascular spaces. (x 200). **C.** Inset of central part of the defect showing larger vascular spaces (VS) and appearance of several layers of mesenchymal connective tissue (MCT). (x 200). **Treated site (D, E, F): D.** Mature lamellar bone was seen bridging the defect site under the Pr with underlying large vascular spaces (VS). (x 40). **E.** Inset of peripheral edge of the defect margin showing the presence of irregularly shaped Haversian systems (HS) and some wide Haversian canals (HC). (200). **F.** Inset of central part of the defect showing the lamellar bone (LB) formation with the presence of many osteocytes (Oc) inside lacunae. (x 200).

(Fig. 5 D, E, F), a new bone arrangement was detected in the lateral borders of the defect in the form of small and irregular spicules of woven (immature) bone, which encroached towards the center along the large vascular spaces. In the central region of the defect, there was a more thickened periosteum with the appearance of several layers of mesenchymal connective tissue. The underlying surface of the mesenchymal connective tissue contained undifferentiated mesenchymal cells that occupied almost the entirety of the defect area.

At 6 weeks, the defect area of the control site was filled mainly with irregular newly formed woven bone at the borders of the defect. Nearing the center, many large vascular spaces and wider layers of mesenchymal connective tissue were present. However, no evidence of lamellar (mature) bone formation could be seen (Fig. 6 A, B, C). In the defect site filled with the GIMgO NPs, mature lamellar bone was seen bridging the defect under the periosteum, along with the presence of irregularly-shaped Haversian systems, some wide Haversian canals, and the presence of many osteocytes inside their lacunae. Additionally, interconnecting bone trabeculae of woven bone were also present by the lamellar bone with large vascular spaces (Fig. 6 D, E, F).

3.3. Micro-CT results

The micro-CT examination corroborated the histological findings regarding the new bone formation (Fig. 7). After 2 weeks, the defect of the control site appeared radiolucent, which indicated no newly formed bone, while some radiopacity was seen in the defect margins filled with the GIMgO NPs as an indication of new bone formation. At 4 weeks, the bony defect filled with the GIMgO NPs displayed an increased radiopacity, which had begun to connect the two borders of the defect and presented a thin line of callus formation as compared to the control site. On the other hand, at 6 weeks, the site filled with the GIMgO NPs showed an almost radio-opaque area covering the entire defect with an unclear line of demarcation between the regenerated zone and tangential innate bone. In comparison, the control site showed thin areas of regenerated bone fragments with no completed bone bridging.

3.4. Histometric results

The results of histomorphometric analysis were displayed in Fig. 8. The total area (TA) of new bone and connective tissue together (Fig. 8A) showed a marked increase in the tested site (implanted with GIMgO NPs) as compared to the control site after 2 weeks ($P < 0.05$) (5.62 ± 0.18 and 4.92 ± 0.06 mm^2, respectively), after 4 weeks ($P < 0.001$) (8.46 ± 0.15 and 6.14 ± 0.3 mm^2, respectively) and after 6 weeks ($P < 0.001$) (14.16 ± 0.13 and 9.36 ± 0.37 mm^2, respectively). When the total area in the tested site was compared according to the post-operative periods, there was a significant increase at the 4th week as compared to the 2nd week and at the 6th week as compared to the 4th week ($P < 0.001$). Regarding the new bone area (NBA) (Fig. 8B), there was a marked increase in the tested site as compared to the control site at the 2nd week ($P < 0.05$) (2.48 ± 0.07 and 1.84 ± 0.14 mm^2, respectively), 4th week ($P < 0.001$) (5.26 ± 0.14 and 63.22 ± 0.28 mm^2, respectively) and 6th week (8.24 ± 0.18 and 5.68 ± 0.22 mm^2, respectively). When the new bone area in the tested site was compared according to the post-operative periods, there was a significant increase at the 4th week as

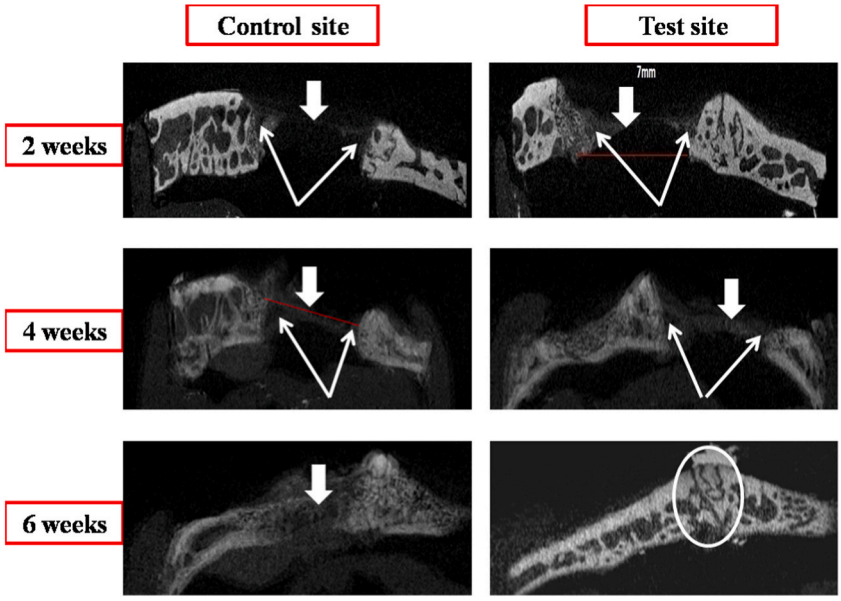

Fig. 7. Micro-CT images of the rabbit's calvarial bone showing the non-implanted (control) site and implanted (test) site with GIMgO NPs. A. After 2 weeks, the defect of control site appeared radiolucent, which indicated no newly formed bone while some radiopacity was seen in the defect margins filled with GIMgO NPsas an indication of new bone formation. **B.** At 4 weeks, the radiopacity increased in the peripheral parts of bony defect filled with GIMgO NPs, connecting the two borders of the defect as compared to the control site. **C.** At 6 weeks, the defect site filled with GIMgO NPs showed an almost radio-opaque area covering the entire defect with unclear boundary between the regenerated area and peripheral native bone. In contrast, the non-filled site showed thin areas of regenerated bone fragments with no completed bone bridging had formed.

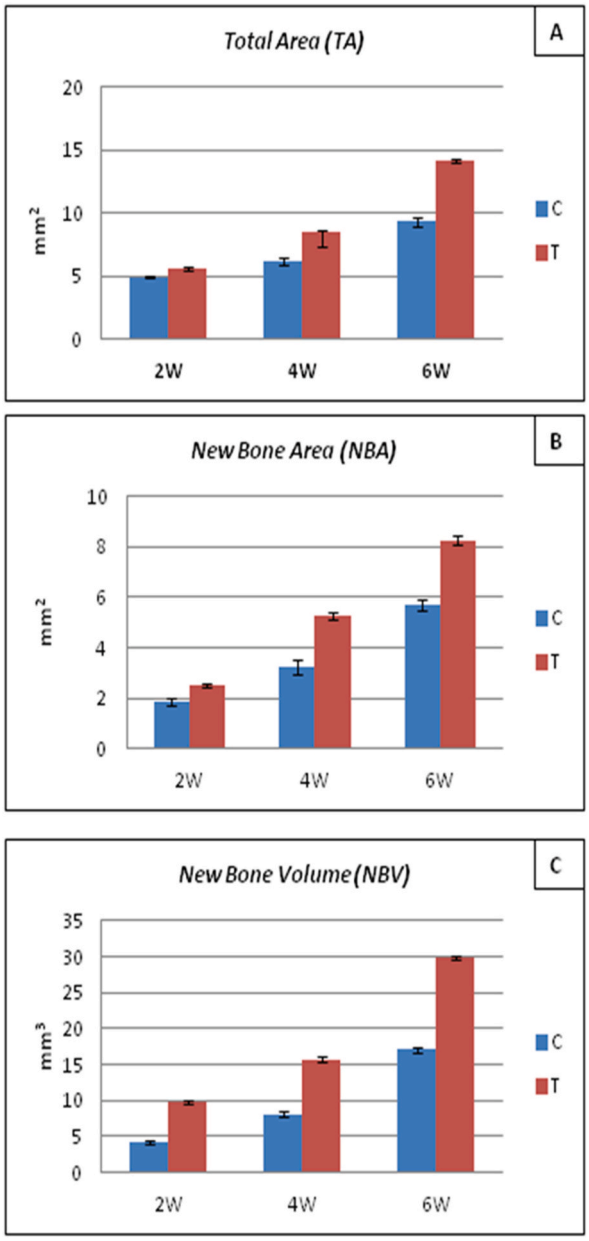

Fig. 8. Graphic representations of statistical analysis of mean values of: A) total area (TA), B) new bone area (NBA) of newly formed bone and C) micro-CT of new bone volume (NBV) at 2, 4 and 6 weeks post-operatively. C = control site (non-implanted). T = test site (implanted with GIMgO NPs).

compared to the 2nd week and at the 6th week as compared to the 4th week ($P < 0.001$).

Regarding the micro-CT analysis of the new bone volume (NBV) (Fig. 8C), there was a significant augmentation ($P < 0.001$) in the test site in comparison to control site after 2 weeks (9.75 ± 0.19 and 4.12 ± 0.23 mm^3, respectively), after 4 weeks (15.75 ± 0.27 and 8.12 ± 0.34 mm^3, respectively) and after 6 weeks (29.88 ± 0.29 and 29.88 ± 0.29 mm^3, respectively). Moreover, the inter-group comparisons showed a significant difference between the 2nd and 4th weeks, as well as a more significant difference after the 6th week period when compared with 4th week period ($P < 0.001$).

4. Discussion

In this study, we examined the efficacy of a new formulation of GIMgO NPs in promoting bone healing activity in experimentally induced calvarial defects. The motivation behind this research stems from the fact that in some cases of periodontal diseases,

maxillofacial defects, or calvarial traumas, the bone gradually loses its functionality despite medical and surgical interventions. These issues can be addressed by utilizing grafting materials, specific bio-membranes, or biomaterials to stimulate the osteogenic properties of bone. However, most of these procedures come with significant limitations and disadvantages, and often exhibit unpredictable rates of resorption, which can considerably impact the amount of bone formation [35–37].

In the present study, the glycerol was incorporated with MgO NPs in an attempt to support their bone healing effects. Previous reports have indicated that the addition of glycerol to dematerialized freeze-dried bone xenografts yielded comparable osseous regeneration in a rat calvarium defect model, as compared to using glycerol alone [38]. Furthermore, clinical evidence has shown that the use of glycerol for bone hydration eliminates the need for additional moisturizers, preserves bone structures, and maintains their biomechanical properties. Its small molecular weight allows it to penetrate tissue structures, replacing water molecules [39]. Glycerol has three hydroxyl groups that are responsible for its water dissolvable and hygroscopic complexion [40,41]. Hygroscopy is the material's capacity to captivate and grasp water around it. Thereupon, the entrapped water in the material modifies its physical properties (e.g. volume and tackiness) [42,43]. As a result of the moisturizing property of glycerol, bone grafts can be safely stored without drying at room temperature [44,45]. This is what promoted its use as a carrier in bone reconstruction matrices for almost twenty years. It was classified by the FDA as a safe and biodegradable liquid. Additionally, it has been used by numerous cosmetic and pharmaceutical manufactures [46].

Dispersion is a vital quality as it affects the physicochemical properties of NPs. The use of ultrasound sonication helps the dispersion of the NPs in the liquid and prevents their agglomeration. Thus, the sonicated GIMgO NPs may have increased the dissemination of the MgO NPs, improving their homogeneity, stability, and bioavailability, by enhancing the pharmacokinetics and pharmacodynamics through continuously hydrating the bone cells. This in turn provided specifically and selectively targeted, controlled osteogenesis [47,48].

The newly formulated hybrid material was characterized using Fourier Transform Infrared Spectroscopy (FTIR) and X-Ray Diffraction analysis (XRD). These analytical techniques are effective in providing information on the composition and interactions of materials, thereby establishing a fundamental understanding of the interaction mechanisms. The FTIR and XRD characterization of GIMgO NPs confirmed the formation of a new hydrogel while maintaining the main structure and characteristics of MgO NPs and glycerol. Previous in vitro and in vivo investigations on NPs have reported that the results depend on various factors such as particle size, distribution, shape, aggregation, and surface charge of NPs. These factors need to be considered in order to analyze the possible hazards associated with the NPs [49,50].

We investigated the osteogenic efficiency of GIMgO NPs by creating critical-size calvarial defects (7 mm in diameter) in rabbits. A critically-sized defect refers to a defect that does not heal naturally and requires additional surgical intervention, such as autologous bone grafting [51,52]. However, the treatment approach should be individualized based on the size and extent of each defect, and with consideration for all available options [53]. Furthermore, this model is commonly utilized in bone investigations to evaluate osteo-promotive materials due to its cost-effective and straightforward approach to assess bone growth processes [54]. Various bones, including the mandible, calvarium, femur, tibia, fibula, and radius, have been used to create defects in animal studies. However, calvarial defects offer conditions similar to other cranial bones [55]. Bone tissue typically exists at the nanometer scale and consists of water, calcium, hydroxyapatite, and proteins. Therefore, the GIMgO NPs hydrogels can mimic the matrix of human bone [56], and the release of MgO NPs can stimulate bone regeneration [57].

Magnesium, an important mineral and the fourth most common metal element found in the human body, is present in bone tissue, accounting for nearly 50% of the total amount in the body [58]. In this regard, MgO is widely recognized for its involvement in the calcification process by stimulating the proliferation and differentiation of osteoblasts, thereby improving osteogenesis [59]. This makes it a promising material for the treatment of bone-related disorders such as osteoporosis, osteomyelitis, and bone fractures. The small size of MgO NPs ($<$100 nm) allows them to bypass biological barriers. The therapeutic effect of the MgO NPs is attributed to other physicochemical properties, including surface area to volume ratio, as well as their mechanical and optical properties [60,61]. Additionally, Mg is entangled in bone transformation, as it activates osteoblasts, enhancing their proliferation and aids in preventing bone resorption [62]. Recently, research has shown that it is imperative to take Mg supplements along with calcium and vitamin D to maintain healthy bones and prevent osteoporosis and fractures associated with osteoporosis [63].

Some previous studies that utilized MgO NPs in composites with biodegradable polymers for bone regeneration applications have confirmed their vital roles in influencing the behavior of the materials' cells [64]. Moreover, the incorporation of MgO NPs into scaffold materials used in bone tissue engineering has demonstrated a significant enhancement in the bioactivity of the scaffold material, enabling it to promote the highest level of bone mineralization [23].

Our histological findings revealed distinct results between the tested and control sites, where the extent of new bone formation exhibited a direct correlation with the post-operative follow-up period, demonstrating a gradual increase from 2 weeks to 4 weeks and from 4 weeks to 6 weeks. At the 2-week mark post-operation, the bony defect of the tested site implanted with GIMgO NPs exhibited closure through the thickened periosteum along with the limited formation of woven (young) bone at the marginal edges of the defect. Conversely, no new bone formation was observed in the control site. It has been reported that the periosteum serves as a crucial source of nutrition and protection for cortical bone [65]. Additionally, the periosteum plays a vital role in prenatal and postnatal bone development and regeneration as it harbors progenitor cells [60]. Furthermore, it has been documented that traumatic or surgical irritation of the periosteum triggers new bone deposition [66,67].

At 4 weeks, the bony defect of the tested site was gradually filled by more proliferation of the periosteum as well as more formation of woven (young) bone that was continuous from the defect margin. This proliferation started from the periosteal membrane, and there was an immense formation of mesenchymal connective tissue that contained undifferentiated mesenchymal cells in addition to many small vascular spaces [68]. It has been suggested that the new bone formation at the border could be attributed to the presence of the

calvarial diploic region with its potent osteogenic effect, as well as its abundant supply of nutrition and stem cells. Furthermore, the newly formed bone exhibited small amounts of bone marrow space [69]. In comparison, the control site presented with vascular spaces and connective tissue, but no evidence of new bone formation.

After 6 weeks, the defect area of the tested site was gradually healed with evidence of new bone trabeculae bridging over the entire defect. The new bone formation was characterized by an arrangement of woven bone in the beginning followed by an organization of lamellar bone. The increased number of osteon and Haversian canals formations was seen in the newly formed bone in the GIMgO NPs sites as compared with the control sites. It was mentioned previously that the initiation of osteoid formation indicated its future transformation into mature bone [70]. These results are consistent with a previous study that assessed bone regeneration after 4 and 8 weeks in calvaria defects in rabbits, revealing new bone deposition and healing at these time points [68]. Moreover, researchers determined 2–4 weeks and 8–12 weeks to be the early and late time periods respectively to observe healing effects in bone [30]. It was reported that when approaching the center of healing bone, osteoblasts that are formed from undifferentiated mesenchymal cells become aligned in a matrix of woven bone. After the formation of sufficient primary woven bone by osteoblasts, a noticeable variation in bone deposition arrangement occurs. The linearly aligned osteoblasts accumulate the collagen matrix in order to make parallel lamellar bone fibers [71].

We evaluated the newly formed bone using micro-CT imaging. It was stated that the two-dimensional and three-dimensional micro-CT analyses are the most reliable methods for measuring the amount of new bone. Hence, the accurate and detailed micro-CT analysis is complimentary to the microscopic examination [72,73]. In our study, micro-CT results were consistent with the histological examinations presented. After two weeks, the results indicated that the tested defects had little bone formation at the peripheral borders and there was no notable variation in newly formed bone volume at the different sites. After four weeks, when compared to the control site, the original bone defects of the tested site were found to have reduced, and the appearance of more new bone formation at the margins extending towards the center could be noted. The area of new bone tissue on the experimental side was much larger than the control site as analyzed by the micro-CT. With the time extension, the relative bone volume gradually increased, providing a statistically significant difference among the different time points. In line with our findings, a previous study by Tsunori, K. et al. [74] found a notable variation in bone volume among the control and the treated groups after 8 weeks using micro-CT interpretation.

5. Conclusion

From the histological and micro-CT results of this study, we could conclude that the locally administered GIMgO NPs formulation was effective in stimulating bone formation and has the potential of healing bone defects, with more significant effects observed over an extended period. Therefore, this formulation can be appropriate for clinical application as an efficient therapeutic substitute to promote bone healing, particularly large bony defects. However, further trials must be performed to assess the reliability of this new formulation regarding the dosing and timing needed for complete healing.

Declarations

Ethical approval and consent to participate

This study was registered at the Unit of biomedical Ethics Research Committee in the Faculty of Medicine, King Abdul-Aziz University (Ref. No. 683-19).

Funding

This research was funded by Deanship of Scientific Research (DSR), King Abdulaziz University, Jeddah, Saudi Arabia, under grant No. (438-254-1439). The authors gratefully acknowledge DSR technical and financial support.

Author contribution statement

Ghada Hussein Naguib, BDS, MSD, MPHE, DSc.; Amr Bayoumi; Abdulghani I Mira; Mohamed T Hamed: Conceived and designed the experiments; Performed the experiments; Analyzed and interpreted the data; Contributed reagents, materials, analysis tools or data; Wrote the paper.

Gamal S. Abd El-Aziz; Ahmad Al-Mehmady; Ali Habib Akbar: Performed the experiments; Analyzed and interpreted the data; Contributed reagents, materials, analysis tools or data; Wrote the paper.

Data availability statement

Data will be made available on request.

Declaration of competing interest

The authors declare that they have no known competing financial interests or personal relationships that could have appeared to influence the work reported in this paper.

Acknowledgements

Acknowledgements are given to Jumana Mazhar for copyediting.

References

[1] Ho Shui, A.B.J. Ling, L.E. Rustom, A.W. Johnson, F.P. Luyten, C. Picart, Bone regeneration strategies: engineered scaffolds, bioactive molecules and stem cells current stage and future perspectives, Biomaterials 180 (2018) 143–162.
[2] Tella, S. H. a. J. C. G, Prevention and treatment of postmenopausal osteoporosis, J. Steroid Biochem. Mol. Biol. 142 (2014) 155–170.
[3] H. Jiao, E. X, D.T. Graves, Diabetes and its effect on bone and fracture healing, Curr. Osteoporos. Rep. 13 (5) (2015) 327–335.
[4] P. Baldwin, D.J. Li, D.A. Auston, H.S. Mir, R.S. Yoon, K.J. Koval, Autograft, allograft, and bone graft substitutes: clinical evidence and indications for use in the setting of orthopaedic trauma surgery, J. Orthop. Trauma 33 (2019) 203–213.
[5] C.E. Gillman, A.C. Jayasuriya, FDA-approved bone grafts and bone graft substitute devices in bone regeneration, Mater. Sci. Eng. C 130 (2021), 112466.
[6] A.L. Matichescu A, L. Rusu, D. Craciun, E.A. Bratu, M. Babucea, M. Leretter, Advanced biomaterials and techniques for oral tissue engineering and regeneration—a review, Materials 13 (22) (2020) 5303.
[7] R.Y.R. Zhao, P.R. Cooper, Z. Khurshid, A. Shavandi, J. Ratnayake, Bone grafts and substitutes in dentistry: a review of current trends and developments, Molecules 26 (2021 2021) 1–27.
[8] D.C. Lobb, B.R. DeGeorge, A.B. Chhabra, Bone graft substitutes: current concepts and future expectations, J. Hand Surg. 44 (2019) 497–505.e2.
[9] H.S. Sohn, J.K. Oh, Review of bone graft and bone substitutes with an emphasis on fracture surgeries, Biomater. Res. 23 (2019) 9.
[10] G. Chandra, A. Pandey, Biodegradable bone implants in orthopedic applications: a review, Biocybern. Biomed. Eng. 40 (2) (2020) 596–610.
[11] P. Kazimierczak, C. Przekora, Osteoconductive and osteoinductive surface modifications of biomaterials for bone regeneration: a concise review, Coatings 10 (10) (2020) 971.
[12] J.G. Lyons, M.A. Plantz, W.K. Hsu, E.L. Hsu, S. Minardi, Nanostructured biomaterials for bone regeneration, Front. Bioeng. Biotechnol. 8 (2020) 922.
[13] N.M. Citakovi'c, Physical properties of nanomaterials, Encycl. Nanosci. Nanotechnol. 67 (2019) 159–171.
[14] S.P. Patil, V.V. Burungale, 2-Physical and chemical properties of nanomaterials, in: N.D. Thorat, J. Bauer (Eds.), Nanomedicines for Breast Cancer Theranostics, Micro and Nano Technologies, Elsevier, Amsterdam, The Netherlands, 2020, pp. 17–31.
[15] N. Joudeh, D. Linke, Nanoparticle classification, physicochemical properties, characterization, and applications: a comprehensive review for biologists, J. Nanobiotechnol. 20 (2022) 262.
[16] Q. Wang, J. Y, J. Yang, B. Li, Nanomaterials promise better bone repair, Mater. Today 19 (8) (2016) 451–463.
[17] J. Girón, E. Kerstner, T. Medeiros, L. Oliveira, G.M. Machado, C.F. Malfatti, P. Pranke, Biomaterials for bone regeneration: an orthopedic and dentistry overview, Braz. J. Med. Biol. Res. 54 (9) (2021), e11055.
[18] Y. Li, Y. Yang, Y. Qing, R. Li, X. Tang, D. Guo, Y. Qin, Enhancing ZnO-NP antibacterial and osteogenesis properties in orthopedic applications: a review, Int. J. Nanomed. 15 (2020) 6247–6262.
[19] M.P. Nikolova, M.S. Chavali, Metal oxide nanoparticles as biomedical materials, Biomimetics 5 (2) (2020 Jun) 27.
[20] N.S. Mahmoud, H.H. Ahmed, M.R. Mohamed, K.S. Amr, A. Hadeer, , Aglan, Ali MAM, M.A. Tantawy, Role of nanoparticles in osteogenic differentiation of bone marrow mesenchymal stem cells, Cytotechnology 72 (1) (2020 Feb) 1–22.
[21] H.A. Naguib G, F. Al-Hazmi, M. Kurakula, A. Al-Dharrabh, H. Alkhalidi, et al., Zein based magnesium oxide nanowires: effect of anionic charge on size, release and stability, Dig. J. Nanomater. Biostruct. (12) (2017) 741–749.
[22] H.K. Naguib Gh, A.H. Hassan, F. Al Hazmi, A. Al Dharrab, H.M. Alkhalidi, et al., Zein based magnesium oxide nanoparticles: assessment of antimicrobial activity for dental implications, Pak. J. Pharm. Sci. (31) (2018) 245–250.
[23] H.S. Roh, et al., Addition of MgO nanoparticles and plasma surface treatment of three-dimensional printed polycaprolactone/hydroxyapatite scaffolds for improving bone regeneration, 2017, Mater. Sci. Eng. C Mater. Biol. Appl. 74 (2017) 525–535.
[24] D. Ke, S. Tarafder, S. Vahabzadeh, S. Bose, Effects of MgO, ZnO, SrO, and SiO2 in tricalcium phosphate scaffolds on in vitro gene expression and in vivo osteogenesis, Mater. Sci. Eng. C 96 (2019) 10–19.
[25] M. Khandaker, Y. Li, T. Morris, Micro and nano MgO particles for the improvement of fracture toughness of bone-cement interfaces, J. Biomech. 46 (5) (2013) 1035–1039.
[26] H. Zhou, B. Liang, H. Jiang, Z. Deng, K. Yu, Magnesium-based biomaterials as emerging agents for bone repair and regeneration: from mechanism to application, J. Magnesium Alloys 9 (3) (2021) 779–804.
[27] S. Su, P.M. Kang, Recent advances in nanocarrier-assisted therapeutics delivery systems, Pharmaceutics 12 (9) (2020 Sep) 837.
[28] C. Nickel, J. Angelstorf, R. Bienert, C. Burkart, S. Gabsch, S. Giebner, A. Haase, B. Hellack, H. Hollert, K. Hund-Rinke, Dynamic light-scattering measurement comparability of nanomaterial suspensions, J. Nanoparticle Res. 16 (2) (2014) 1–12.
[29] T.R. Ray, B. Lettiere, J. de Rutte, S. Pennathur, Quantitative characterization of the colloidal stability of metallic nanoparticles using UV–Vis absorbance spectroscopy, Langmuir 31 (12) (2015) 3577–3586.
[30] P.J. Sohn Jy, Y.J. Um, U.W. Jung, C.S. Kim, K.S. Cho, S.H. Choi, Spontaneous healing capacity of rabbit cranial defects of various sizes, J. Periodontal. Implant Sci. 40 (2010) 180–187.
[31] C.-G.J. Delgado-Ruiz Ra, G.E. Romanos, Critical size defects for bone regeneration experiments in rabbit calvariae: systematic review and quality evaluation using ARRIVE guidelines, Clin. Oral Implants Res. 26 (2015) 915–930.
[32] L.C. Bancroft J, The hematoxylin and eosin, in: S.K. Suvarna, C. Layton, J.D. Bancroft (Eds.), Theory & Practice of Histological Techniques, seventh ed., Churchill Livingstone of El Sevier, Philadelphia, 2013, pp. 172–214. Ch. 10 - 11).
[33] S.S. Hagar S, Y. Mona, M. Nancy, Histomorphometric and histological evaluations of the simvastatin effect on alveolar bone loss induced by cyclosporine A in rats, Indian J. Multidiscip. Dent. 5 (1) (2015) 2–9.
[34] K.A. Hong I, H.C. Pae, J.K. Cha, J.S. Lee, J.W. Paik, et al., Distinctive bone regeneration of calvarial defects using biphasic calcium phosphate supplemented ultraviolet-crosslinked collagen membrane, J. Periodontal. Implant Sci. 50 (2020) 14–27.
[35] M.A. Soares Lg, A.F. Barbosa, et al., Raman study of the repair of surgical bone defects grafted with biphasic synthetic microgranular HA C b-calcium triphosphate and irradiated or not with λ780 nm laser, Laser Med. Sci. 29 (2014) 1539–1550.
[36] U.N. Arima Y, Y. Hashimoto, et al., Evaluation of bone regeneration by porous alpha-tricalcium phosphate/atelocollagen sponge composite in rat calvarial defects, Orthod. Waves 72 (2013) 23–29.
[37] P.J. Bezerra Bt, F.E.D. Figueiredo, J. Brandao, L.C.G. Ayres, L.C.F. da Silva, Autogenous bone graft versus bovine bone graft in association with plateletrich plasma for the reconstruction of alveolar clefts: a pilot study, Cleft Palate Craniofac. J. 56 (1) (2019) 134–140.
[38] M.J. Matzenbacher Sa, J.C. McPherson, M.F. Cuenin, S.D. Hokett, M. Sharawy, M.E. Peacock, In vivo effectiveness of a glycerol-compounded demineralized freeze-dried bone xenograft in the rat calvarium, J. Periodontol. 74 (2003) 1641–1646.
[39] T. Yamada, A. Habuka, I. Hatta, Moisturizing mechanism of glycerol and diglycerol on human stratum corneum studied by synchrotron X-ray diffraction, Int. J. Cosmet. Sci. 43 (1) (2021 Feb) 38–47.
[40] M. Roy, K. DeVoe, A. Bandyopadhyay, S. Bose, Mechanical property and in vitro biocompatibility of brushite cement modified by polyethylene glycol, Mater. Sci. Eng. C 32 (8) (2012) 2145–2152.
[41] A. Vlysidis, M. Binns, C. Webb, C. Theodoropoulos, Glycerol utilisation for the production of chemicals: conversion to succinic acid, a combined experimental and computational study, Biochem. Eng. J. 58 (2011) 1–11.

[42] L. Grech, B. Mallia, J. Camilleri, Investigation of the physical properties of tricalcium silicate cement-based root-end filling materials, Dent. Mater. 29 (2) (2013) e20–e28.
[43] R.S. Graham, B. S, Bs, A. Proffer, M.A. Moore, R.A. Vega, J.M. Stary, B. Mathern, Evaluation of glycerol-preserved bone allografts in cervical spine fusion: a prospective, randomized controlled trial, J. Neurosurg. Spine 22 (2015) 1–10.
[44] S.D. Samsell B, X. Qin, Q. McLean, P. Sohoni, K. Gonzales, Mark A, M.A. Moore, Preservation of allograft bone using a glycerol solution: a compilation of original preclinical research, Biomater. Res. 23 (5) (2019).
[45] D.K. Park, R. Roberts, P. Arnold, D.H. Kim, R. Sasso, K.C. Baker, J.S. Fischgrund, Lumbar spine fusion rates with local bone in posterolateral and combined posterolateral and interbody approaches, JAAOS Global Res. Rev. 3 (11) (2019).
[46] Z.Y. Ben, H. Samsudin, M.F. Yhaya, Glycerol: its properties, polymer synthesis, and applications in starch based films, Eur. Polym. J. (2022), 111377.
[47] R. van der Meel, E. Sulheim, Y. Shi, F. Kiessling, W.J. Mulder, T. Lammers, Smart cancer nanomedicine, Nat. Nanotechnol. 14 (11) (2019) 1007–1017.
[48] M.J. Mitchell, M.M. Billingsley, R.M. Haley, M.E. Wechsler, N.A. Peppas, R. Langer, Engineering precision nanoparticles for drug delivery, Nat. Rev. Drug Discov. 20 (2) (2021) 101–124.
[49] J. Jiang, G. Oberdörster, P. Biswas, Characterization of size, surface charge, and agglomeration state of nanoparticle dispersions for toxicological studies, J. Nanoparticle Res. 11 (1) (2009) 77–89.
[50] J.S. Taurozzi, V.A. Hackley, M.R. Wiesner, Ultrasonic dispersion of nanoparticles for environmental, health and safety assessment–issues and recommendations, Nanotoxicology 5 (4) (2011) 711–729.
[51] D.W. Sanders, M. Bhandari, G. Guyatt, D. Heels-Ansdell, E.H. Schemitsch, M. Swiontkowski, P. Tornetta III, S. Walter, S. Investigators, Critical-sized defect in the tibia: is it critical? Results from the SPRINT trial, J. Orthop. Trauma 28 (11) (2014) 632–635.
[52] A. Nauth, E. Schemitsch, B. Norris, Z. Nollin, J.T. Watson, Critical-size bone defects: is there a consensus for diagnosis and treatment? J. Orthop. Trauma 32 (2018) S7–S11.
[53] M.N. Vajgel A, B.C. Farias, A. Petrie, R. Cimoes, N. Donos, A systematic review on the critical size defect model, Clin. Oral Implants Res. 25 (2014) 879e93.
[54] H.V. Kim S, M. Kashif, D. Jeong, G. Kim, Evaluation of Bone Regeneration on Polyhydroxyethyl-polymethyl Methacrylate Membrane in a Rabbit Calvarial Defect Model In Vivo, 30, (5), 2016, pp. 587–591.
[55] P.N.T. Pripatnanont, S. Vongvatcharanon, K. Phurisat, The primacy of platelet-rich fibrin on bone regeneration of various grafts in rabbit's calvarial defects, J. Cranio-Maxillo-Fac. Surg. 41 (8) (2013), e191ee200.
[56] Z.Z.J. Wang, W. Tang, L. Hu, X. Chen, Y. Su, C. Zou, J. Wang, W.W. Lu, W. Zhen, Multifunctional nanoengineered hydrogels consisting of black phosphorus nanosheets upregulate bone formation, Small 15 (2019), e1901560.
[57] E. Piantanida, A. G, A. Bertucci, L. De Cola, Design of nanocomposite injectable hydrogels for minimally invasive surgery, Acc. Chem. Res. 52 (2019) 2101–2112.
[58] A. Mahapatro, T. Matos Negron, A. Gomes, Nanostructured self assembled monolayers on magnesium for improved biological performance, Mater. Technol. 31 (13) (2016) 818–827.
[59] A. Saboori, M. R, F. Moztarzadeh, M. Sheikhi, M. Tahriri, M. Karimi, Synthesis, characterization and in vitro bioactivity of sol-gel-derived SiO2–CaO–P2O5–MgObioglass, Mater. Sci. Eng. C 29 (2009) 335–340.
[60] I. Khan, K. Saeed, I. Khan, Review nanoparticles: properties, applications and toxicities, Arab. J. Chem. 12 (2) (2019) 908–931.
[61] K. Zheng, J. Xie, Engineering ultrasmall metal nanoclusters as promising theranostic agents, Trends Chem. 2 (7) (2020) 665–679.
[62] C. Janning, E. Willbold, C. Vogt, J. Nellesen, A. Meyer-Lindenberg, H. Windhagen, F. Thorey, F. Witte, Magnesium hydroxide temporarily enhancing osteoblast activity and decreasing the osteoclast number in peri-implant bone remodelling, Acta Biomater. 6 (5) (2010) 1861–1868.
[63] S. Galli, Y. Naito, J. Karlsson, W. He, M. Andersson, A. Wennerberg, R. Jimbo, Osteoconductive potential of mesoporous titania implant surfaces loaded with magnesium: an experimental study in the rabbit, Clin. Implant Dent. Relat. Res. 17 (6) (2015) 1048–1059.
[64] D.J. Hickey, et al., Adding MgO nanoparticles to hydroxyapatite-PLLA nanocomposites for improved bone tissue engineering applications, Acta Biomater. 14 (2015) 175–184.
[65] Z.F.A. Lin, D.M. Salem, G. Intini, Periosteum: biology and applications in craniofacial bone regeneration, 2014, J. Dent. Res. 93 (2014) 109–116.
[66] H.K.T.M. Chang, Concise review: the periosteum: tapping into a reservoir of clinically useful progenitor cells, Stem Cells Trans. Med. 1 (2012) 480–491.
[67] M.M. Zakaria O, S. Kasugai, A novel osteogenesis technique: the expansible guided bone regeneration, J. Tissue Eng. 3 (2012), 2041731412441194.
[68] S.T. Gosain Ak, L.S. Song, C.C. Capel, P.V. Sudhakar, H.S. Matloub, Osteogenesis in calvarial defects: contribution of the dura, the pericranium, and the surrounding bone in adult versus infant animals, Plast. Reconstr. Surg. 112 (2003) 515e27.
[69] F.K. Inoue S, M. Matsuki-Fukushima, M. Nakamura, Repair processes of flat bones formed via intramembranous versus endochondral ossification, J. Oral Biosci. 62 (1) (2020) 52–57.
[70] T.S. Bose S, S.S. Banerjee, N.M. Davies, A. Bandyopadhyay, Understanding in vivo response and mechanical property variation in MgO, SrO and SiO2 doped b-TCP, Bone 48 (2011) 1282–1290.
[71] W.J. Shapiro F, Woven bone overview: structural classification based on its integral role in developmental, repair and pathological bone formation throughout vertebrate groups, Eur. Cell. Mater. 38 (2019) 137–167.
[72] K.D.M. Laperre, N. van Gastel, S. Torrekens, K. Moermans, R. Bogaerts, F. Maes, G. Carmeliet, Development of micro-CT protocols for in vivo follow-up of mouse bone architecture without major radiation side effects, Bone 49 (2011) 613–622.
[73] al , H. e, Early clinical applications for imaging at microscopic detail: microfocus Computed Tomography (micro-CT), Br. J. Radiol. 90 (1075) (2017), 20170113.
[74] K. Tsunori, S. Sato, A. Hasuike, S. Manaka, H. Shino, N. Sato, M. Miyazaki, Effects of intermittent administration of parathyroid hormone on bone augmentation in rat calvarium, Implant Dent. 24 (2015) 142–148.